

See discussions, stats, and author profiles for this publication at: <https://www.researchgate.net/publication/336162588>

Prediction of the Flow Response of a Turbulent Flame to Acoustic Perturbations Based On Mean Flow Resolvent Analysis

Article in *Journal of Engineering for Gas Turbines and Power* · September 2019

DOI: 10.1115/1.4044993

CITATIONS

9

READS

302

3 authors:



Thomas Ludwig Kaiser

Technische Universität Berlin

20 PUBLICATIONS 83 CITATIONS

[SEE PROFILE](#)



Lutz Lesshaft

CNRS / Ecole Polytechnique

68 PUBLICATIONS 1,092 CITATIONS

[SEE PROFILE](#)



Kilian Oberleithner

Technische Universität Berlin

147 PUBLICATIONS 2,074 CITATIONS

[SEE PROFILE](#)

Some of the authors of this publication are also working on these related projects:



Thermoacoustic Instabilities [View project](#)



Reduced-Order Modeling [View project](#)

PREDICTION OF THE FLOW RESPONSE OF A TURBULENT FLAME TO ACOUSTIC PERTUBATIONS BASED ON MEAN FLOW RESOLVENT ANALYSIS

Thomas Ludwig Kaiser*

Laboratory for Flow Instabilities
 and Dynamics
 Technische Universität Berlin,
 Müller-Breslau-Straße 8,
 10623 Berlin, Germany
 Email: t.kaiser@tu-berlin.de

Lutz Lesshafft

Laboratoire d'Hydrodynamique
 CNRS / École polytechnique
 91128 Palaiseau, France

Kilian Oberleithner

Laboratory for Flow Instabilities
 and Dynamics
 Technische Universität Berlin,
 Müller-Breslau-Straße 8,
 10623 Berlin, Germany

ABSTRACT

Resolvent analysis is applied to a non-reacting and a reacting swirled jet flow. Time-averaged flows as input for the resolvent analysis and validation for the results of the resolvent analysis are obtained by experiments. We show that in the non-reacting (cold) flow case, the resolvent analysis is capable of predicting the hydrodynamic response to upstream harmonic acoustic forcing if the flow shows low-rank behavior. This is the case for low and moderate acoustic forcing amplitudes. Even for very strong acoustic velocity amplitudes, that are of the same order of magnitude as the flow velocity, the resolvent analysis still provides reasonable results. The method also yields very good results for the reacting flow in terms of velocity fluctuation and heat release response to the acoustic forcing. This confirms the idea that the resolvent method could be applied to estimate the Flame Transfer Function based on the mean flow and flame.

p Pressure
 Re Reynolds number
 t Time
 T Temperature
 u Velocity
 U Characteristic velocity

Greek:

δ Kronecker delta
 μ^2 Gain
 ν Viscosity
 Φ Optimal forcing
 Ψ Optimal response
 ρ Density
 ω Circular frequency

Superscripts:

$\langle \cdot \rangle$ Coherent fluctuation
 $\langle \cdot \rangle$ Fourier transform
 $\langle \cdot \rangle'$ Stochastic fluctuation
 $\langle \cdot \rangle$ Time-average
 $\langle \cdot \rangle^T$ Transpose

Subscripts:

$\langle \cdot \rangle_a$ Acoustic
 $\langle \cdot \rangle_b$ Bulk
 $\langle \cdot \rangle_e$ Eddy

NOMENCLATURE

Latin:

a Thermal diffusivity
 D Characteristic length
 K Turbulent kinetic energy
 \mathbf{n} Normal vector
 Pr Prandtl number

*Address all correspondence to this author.

$\langle \cdot \rangle_r$ Radial
 $\langle \cdot \rangle_t$ Azimuthal
 $\langle \cdot \rangle_z$ Axial

1 INTRODUCTION

In the reactive flow of a combustion engine, the dynamics of the flow are of immense importance, and can have either beneficial (e.g. mixing and fuel atomization [1, 2]) or negative (e.g. combustion instabilities [3]) effects. Due to their diversity and complexity, comprehending their formation process has been a difficult challenge, not only in reactive flows.

In order to further their understanding, Linear Stability Analysis (LSA) has been applied to understand the feedback mechanisms of self-sustained instabilities. This method uses the time-averaged flow and analyzes the temporal evolution of modal structures in the flow. Barkley et al. [4] for example showed that a BiGlobal LSA correctly reproduces the dynamical structures of the famous von Kármán vortex street evolving in the wake of a cylinder. Also for swirling jets – a configuration of special interest to combustion engineers and scientists – local LSAs showed that the phenomenon of Precessing Vortex Cores (PVCs) is well reproduced by this analysis (see e.g. Terhaar et al. [5]). Local approaches, which rely on a parallel flow assumption, however are hardly applicable to industrial geometries. Tammiola and Juniper [6] and Kaiser et al. [7] therefore extended the approach to industrial geometries by applying BiGlobal stability analysis to swirled industrial injection systems. LSA has been proven to give valuable insight into the cause and nature of the PVC, as well as insight into efficient methods for the control of global instabilities. At the same time, the method is numerically cheap in comparison with large scale flow simulations.

Nevertheless, the method of modal LSA analysis has limits. While it gives insight into the mechanisms of intrinsic instabilities, the method fails to describe growth and decay of perturbations triggered by external forcing. This effect however is highly important for many applications (e.g. actuation of coherent fluctuations due to turbulence [8], energy conversion from acoustics to hydrodynamics [9, 10]). Furthermore, non-modal growth (see e.g. [8]) is not taken into account in modal LSA.

A promising method which takes these effects into account is an analysis of the resolvent operator, linearized around the time-averaged flow. This method was first applied to hydrodynamics by Trefethen et al. [11], who analyzed non-modal growth of Poiseuille and Couette flow. Briefly stated, a Singular Value Decomposition (SVD) of the resolvent operator yields the orthonormal basis of optimal forcings, Ψ_j (left singular vectors), and their corresponding responses Φ_j (right singular vectors), where the singular values, μ_j^2 , correspond to the gain, for example in terms of kinetic energy (L^2 norm; see e.g. Beneddine et

al. [12]):

$$\mu_j^2 = \frac{\|\Phi_j\|_r^2}{\|\Psi_j\|_f^2}. \quad (1)$$

It was shown by McKeon and Sharma [13], that if one singular value of the resolvent operator is of significantly higher magnitude than the remaining singular values, the respective optimal response dominates the dynamics around the mean flow. This is also known as low-rank behavior.

Although the method has proven to yield valuable understanding of dynamical structures in various configurations, its applicability in combustion research and engineering remains an open topic. Since the method in theory is capable of describing the dynamics in a system with nothing else as input than the time-averaged flow quantities, it might not only be capable to describe fluctuations of the flow, but also of the heat release, if the flame is properly modeled in the approach. This signifies that instead of measuring the Flame Transfer Function (FTF) by experimental [14] or numerical [15, 16] means, this method should be able to estimate an FTF of a flame, when only the time-average of the flow is provided. While current analytical models for description of the FTF are based on kinematic descriptions of the flame (see Fleifil et al. [17] and Schuller et al. [18]) and are restricted to laminar flames, the proposed approach could also be used for turbulent flames, similar to what has been done for turbulent non-reacting jets (Schmidt et al. [19] and Lesshafft et al. [20]). The FTFs, which describes a flame's response to acoustic forcing in terms of heat release fluctuations, can then be used in order to model thermoacoustic instabilities by closing the Helmholtz equation (see e.g. Silva et al [21]) or a network model (see e.g. Schurmanns et al. [22] and Emmert et al. [23]).

In this paper, we apply this analysis method to mean flows measured in a swirl combustor. In this context, the central questions addressed in this paper are the following:

1. Provided a given time-averaged flow, does the resolvent analysis predict the hydrodynamic response of the swirling jet to acoustic forcing, if the dominant gain, μ_1^2 , is of much higher amplitude than the subdominant gains (low rank requirement)?
2. What are the limits of the approach with respect to fluctuation amplitude? Do non-linear effects in the case of strong acoustic forcing decrease the magnitude of the dominant gain, so that the low-rank requirement is no longer met?
3. Is the method applicable to reactive flows? Does it predict heat release fluctuations?

In order to answer these questions, the swirled injection system is acoustically excited from the inlet, and the hydrodynamic response is measured in the experiment by means of Particle Image Velocimetry (PIV) and OH^* -chemiluminescence. The ex-

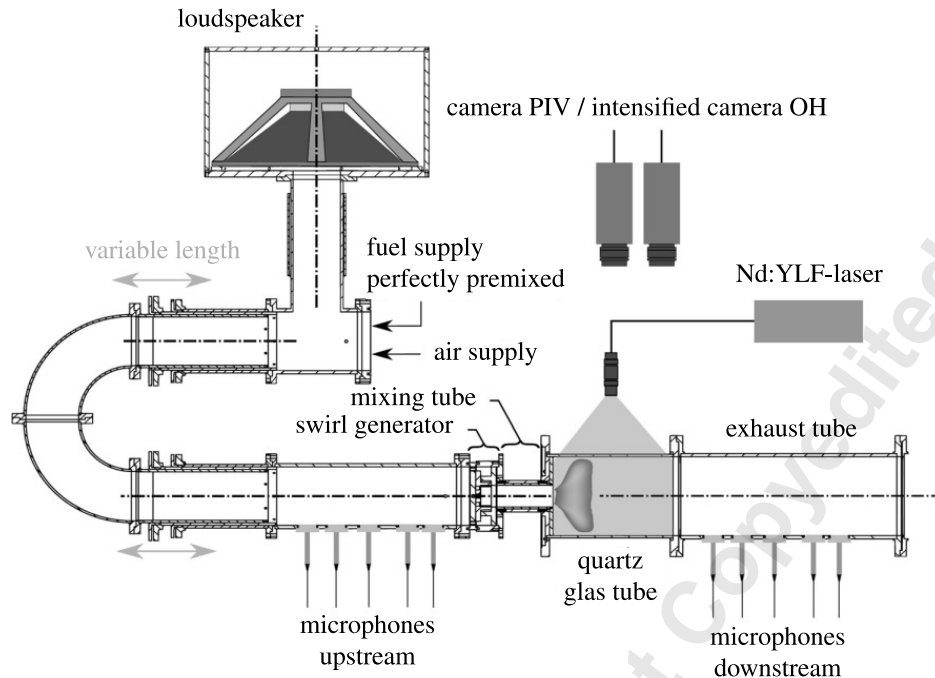


FIGURE 1: Sketch of the experimental set-up

perimental set-up and data acquisition technique is described in Section 2. The mean flow velocities and density measured in the experiment will serve as a basis for the resolvent analysis, which is reviewed together with its numerical implementation in Section 3. In Section 4, the results of the resolvent analysis are discussed and validated against the hydrodynamic response which is measured in the experiment. In the resolvent analysis of the cold flow case, forcing in both the linear (Section 4.1) and in the non-linear regime (Section 4.2) is considered. Furthermore, the results of the resolvent analysis around a reacting-flow are presented in Section 4.3. Finally, Section 5 concludes the results.

2 Experiment

2.1 Experimental Set-Up

A sketch of the experimental set-up is illustrated in Fig. 1. The arrangement corresponds to the one described in Oberleithner et al. [24]. The gas enters the test-rig in its upstream plenum at atmospheric conditions. In the swirl generator, the gas is injected tangentially into the mixing tube, and finally reaches the combustion chamber. More detailed information on the swirler geometry is provided in Reichel et al. [25]. Both non-reacting (air) and reacting flows (methane-air, equivalence ratio 0.7) are considered. The Reynolds number with respect to the diameter of the mixing tube is approximately $Re \approx 60,000$, which corresponds to an air mass flow of $2.78 \cdot 10^{-2} \text{ kg s}^{-1}$.

Loudspeakers, which are mounted in the upstream section

of the test-rig, are used to force the flow by harmonic acoustic waves. The acoustic forcing is conducted at amplitudes in the linear regime, i.e. velocity fluctuations below 10% of the bulk speed, as well as in the non-linear regime of higher amplitudes.

Data Acquisition

Visual access to the combustion chamber is granted by a circular 200 mm quartz glass window. Velocity field, density field and OH-chemiluminescence measurements are recorded simultaneously via two synchronized high speed cameras. PIV measurements yield the velocity fields in the meridional section (see sketch in Fig. 1). Titanium dioxide seeding particles are illuminated by a Quantronix Darwin Duo laser (30 mJ at 1 kHz) and recorded by a Photron Fastcam SA 1.1 high-speed camera (1 Mpixel at 2.7 kHz double frame). At a frame rate of 2000 Hz, 2000 images were recorded for every operating point (gas composition, excitation frequency and excitation amplitude). The PIV snapshots were analyzed by PIVview (PIVTEC GmbH) [26]. This software uses standard digital PIV processing [27], which is enhanced by iterative multigrid interrogation with image deformation [28]. In order to obtain the mean density fields, the Quantitative Light Sheet (QLS) technique is applied [29]. In this method, the light intensity signal from the PIV snapshots is used to calculate the local seeding density, which in turn allows to estimate the fluid density.

A second synchronized Photron Fastcam SA 1.1 camera was used to record simultaneously the OH^{*}-chemiluminescence.

Here, an image intensifier and an optical filter, which restricts the observed wave lengths to the window between 295 – 340 nm, were applied. The OH* signal recorded with the camera was phase-averaged with respect to the acoustic actuation signal and able-deconvoluted in order to get a planar representation of the heat-release rate fluctuations.

3 Resolvent Analysis

3.1 Theory

A reactive flow can be described by the Navier-Stokes momentum equation, the continuity equation, and a transport equation for the internal energy of the fluid. Inserting the triple decomposition [30] for the velocity, pressure and density,

$$\mathbf{u} = \bar{\mathbf{u}} + \tilde{\mathbf{u}} + \mathbf{u}', \quad p = \bar{p} + \tilde{p} + p', \quad \rho = \bar{\rho} + \tilde{\rho} + \rho', \quad (2)$$

where the overbar denotes the temporal mean, the tilde the coherent fluctuation and the prime a stochastic fluctuation, yields a set of first order governing equations for the coherent structures around a linearized mean flow. In the low Mach number limit and in non-dimensional form, this set of equation writes [30, 31]:

$$\begin{aligned} \bar{\rho} \frac{\partial \tilde{\mathbf{u}}}{\partial t} + \bar{\rho} (\tilde{\mathbf{u}} \cdot \nabla) \bar{\mathbf{u}} + \bar{\rho} (\bar{\mathbf{u}} \cdot \nabla) \tilde{\mathbf{u}} + \tilde{\rho} (\bar{\mathbf{u}} \cdot \nabla) \bar{\mathbf{u}} + \langle (\rho \mathbf{u}' \cdot \nabla) \mathbf{u}' \rangle \\ - \overline{(\rho \mathbf{u}' \cdot \nabla) \mathbf{u}'} = \tilde{f} - \nabla \tilde{p} + \frac{1}{\text{Re}} \left(\Delta \tilde{\mathbf{u}} + \frac{1}{3} \nabla (\nabla \cdot \tilde{\mathbf{u}}) \right), \end{aligned} \quad (3)$$

$$\frac{\partial \tilde{p}}{\partial t} + \nabla \tilde{\rho} \cdot \bar{\mathbf{u}} + \nabla \bar{\rho} \cdot \tilde{\mathbf{u}} + \bar{\rho} (\nabla \cdot \tilde{\mathbf{u}}) + \tilde{\rho} (\nabla \cdot \bar{\mathbf{u}}) = 0, \quad (4)$$

and

$$\begin{aligned} \bar{\rho}^3 \nabla \cdot \tilde{\mathbf{u}} + 3\bar{\rho}^2 \tilde{\rho} \nabla \cdot \bar{\mathbf{u}} + \frac{1}{\text{RePr}} (\bar{\rho} \Delta \tilde{p} + \tilde{\rho} \Delta \bar{p} - 4\nabla \tilde{\rho} \nabla \bar{p}) \\ + \langle \nabla \cdot (\rho T' \mathbf{u}') \rangle - \overline{\nabla \cdot (\rho T' \mathbf{u}')} = 0. \end{aligned} \quad (5)$$

Here, t denotes time, and the Reynolds and the Prandtl numbers are defined as

$$\text{Re} = \frac{UD}{\nu}, \quad \text{Pr} = \frac{\nu}{a}, \quad (6)$$

respectively, where $D = 0.034\text{m}$ is the diameter of the mixing tube, $U = 27.4\text{ms}^{-1}$ is the maximum flow speed, ν is the kinematic viscosity, and a corresponds to the thermal diffusivity. The

vector f in the momentum equation stands for the coherent fluctuations of a body force. While temporal averages are denoted by an overbar, the angle brackets in the set of Eqns. (3–5) stand for a phase average. These terms arise from the non-linear terms in the momentum and energy equations. Terms 5 and 6 on the Left Hand Side (LHS) of Eqn. (3) represent stochastic Reynolds stress fluctuations during the period of the coherent structure [32]. In this paper, we model the influence of these stochastic terms on the coherent structures by an eddy viscosity. Since both the velocity fluctuations and the mean velocity fields are known from experimental measurements, the eddy viscosity can be estimated by the Boussinesq approximation [33]. Since this yields six eddy viscosity scalars, one for every independent entry in the Reynolds stress tensor, the least mean squares eddy viscosity based on all terms in the stress tensor is estimated and applied:

$$\nu_e = \frac{\left(-\overline{u'_i u'_j} + \frac{2}{3} K \delta_{ij} \right) \cdot \left(\frac{\partial \bar{u}_j}{\partial x_i} + \frac{\partial \bar{u}_i}{\partial x_j} \right)}{\left(\frac{\partial \bar{u}_k}{\partial x_l} + \frac{\partial \bar{u}_l}{\partial x_k} \right) \cdot \left(\frac{\partial \bar{u}_k}{\partial x_l} + \frac{\partial \bar{u}_l}{\partial x_k} \right)}. \quad (7)$$

Here, for convenience the Einstein notation is applied with the indices, i, j, k and l . This approach yields a spatially varying turbulent Reynolds number, which is based on the sum of molecular viscosity and eddy viscosity. In accordance with various strategies in time integration of governing equations of compressible or low Mach number flows (see e.g. Pope [34] and Poinot and Veynante [35]), non-vanishing terms involving the stochastic fluctuations in the energy equation are modeled by a constant turbulent Prandtl number, which is fixed to 0.9.

Introducing linear operators L, B and P , Eqns. (3–5) can be rewritten as

$$B \frac{\partial}{\partial t} [\tilde{\mathbf{u}}, \tilde{p}, \tilde{\rho}]^T = L [\tilde{\mathbf{u}}, \tilde{p}, \tilde{\rho}]^T + P \tilde{f}. \quad (8)$$

Applying the temporal Fourier transform yields the corresponding equation in frequency space:

$$i\omega B [\hat{\mathbf{u}}, \hat{p}, \hat{\rho}]^T = L [\hat{\mathbf{u}}, \hat{p}, \hat{\rho}]^T + P \hat{f}. \quad (9)$$

The linear operators in Eqn. (9) can be rearranged to provide a link between the forcing term \hat{f} and the response to the forcing $[\hat{\mathbf{u}}, \hat{p}, \hat{\rho}]^T$:

$$\hat{\mathbf{u}} = (i\omega B - L)^{-1} P \hat{f} = \mathfrak{R} \hat{f}. \quad (10)$$

The resolvent operator, \mathfrak{R} , therefore yields the solution of the Linearized Navier-Stokes Equations (LNSE), $\hat{\mathbf{u}}$, when it is applied on a given forcing, \hat{f} . Furthermore, it can be shown (see

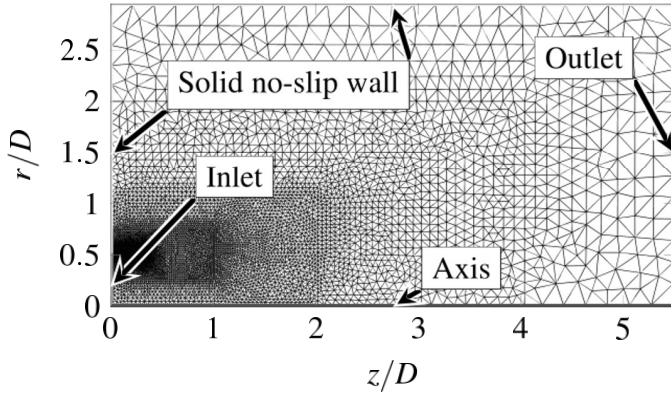


FIGURE 2: Numerical domain and grid for the resolvent analysis

e.g. Sipp et al. [36] or Beneddine et al. [12]) that the right singular vectors and the left singular vectors of the resolvent operator, \mathfrak{R} , correspond to optimal forcings, Φ_j , and optimal responses, Ψ_j , respectively. The energy gain, μ_j^2 , between forcing input and flow response is evaluated in this study as the ratio between their respective norms of velocity fluctuations. The response norm is defined by a volume integral over the entire flow domain Ω , whereas the forcing norm measures only axial velocity forcing in the inlet boundary plane Γ (green line in Fig. 2). This definition of the gain is written as

$$\mu_j^2(\omega) = \frac{\|\Phi_j\|_r^2}{\|\Psi_j\|_f^2} = \frac{\int_{\Omega} |\tilde{\mathbf{u}}|^2 r dr dx}{\int_{\Gamma} |\tilde{u}_x|^2 r dr} \quad (11)$$

When one gain at a given frequency is significantly greater than all remaining values (low-rank condition), then the dynamics of the LNSE can be appropriately approximated by the optimal forcing/response pair which corresponds to the dominant gain [12].

3.2 Numerical Implementation

In order to find the pairs of optimal forcing and response defined by the norms in Eqn. (11), the integral form of the linear operators in Eqn. (10) must be determined. They are obtained by spatial discretization and integration in the domain of interest. Both is performed by the software package FreeFEM++ [37, 38]. Figure 2 shows the numerical domain with an exemplary grid. In the region of highest mesh refinement the mesh size is $\Delta x = 0.23$ mm, which is smaller than the resolution in the PIV data. Table 1 summarizes the applied boundary conditions for the velocity components in radial, azimuthal and axial directions and for pressure and density. In order to increase numerical stability, the Reynolds number is limited by $\text{Re}_{\max} = 5000$.

TABLE 1: Boundary conditions for the perturbations; \mathbf{n} is the normal vector on the boundary.

	Axis	Walls	Inlet	Outlet
radial vel.	$\tilde{u}_r = 0$	$\tilde{u}_r = 0$	$\frac{\partial \tilde{u}_r}{\partial \mathbf{n}} = 0$	$\tilde{u}_r = 0$
azimuthal vel.	$\tilde{u}_t = 0$	$\tilde{u}_t = 0$	$\frac{\partial \tilde{u}_t}{\partial \mathbf{n}} = 0$	$\tilde{u}_t = 0$
axial vel.	$\frac{\partial \tilde{u}_z}{\partial \mathbf{n}} = 0$	$\tilde{u}_r = 0$	$\frac{\partial \tilde{u}_z}{\partial \mathbf{n}} = 0$	$\tilde{u}_z = 0$
pressure	$\frac{\partial \tilde{p}}{\partial \mathbf{n}} = 0$	$\frac{\partial \tilde{p}}{\partial \mathbf{n}} = 0$	$\frac{\partial \tilde{p}}{\partial \mathbf{n}} = 0$	$\tilde{p} = 0$
density	$\frac{\partial \tilde{\rho}}{\partial \mathbf{n}} = 0$	$\frac{\partial \tilde{\rho}}{\partial \mathbf{n}} = 0$	$\frac{\partial \tilde{\rho}}{\partial \mathbf{n}} = 0$	$\tilde{\rho} = 0$

A mesh convergence study confirms that results only change marginally with further refined meshes. The linear operators arranged in FreeFEM++ are imported into Matlab, where the resolvent operator is constructed and the SVD is performed.

4 Results

The experimental measurements yield both the time-averaged flows as input for the resolvent analysis and the spatio-temporal structures of the hydrodynamic response of the flow, which are obtained by an Fast Fourier Transform (FFT) of the experimental snapshots. The time averages are shown in Fig. 3 for the unperturbed cold flow and for the reacting flow case. The mean density field of the latter is displayed in Fig. 4. In both cases, vortex breakdown occurs, marked by an inversion of the flow direction on the jet axis. Nevertheless, the flow is sub-critical with respect to the PVC, and no coherent self-sustained instabilities occur. Note here that in agreement with previous studies (e.g. Oberleithner et al. [39]), we assume that the mean flow in azimuthal direction can be neglected, since the forcing of the jet is axisymmetric. The azimuthal mean velocity is therefore set to 0 ms^{-1} .

In the following, we address the central questions of this paper. In Section 4.1 the resolvent analysis is tested for small acoustic forcing amplitudes. Subsequently, in order to test the applicability limits of the approach, we repeat the analysis for high forcing amplitudes in Section 4.2. And finally, the reacting flow will be examined via resolvent analysis. We expect here, that the method is able to reproduce the hydrodynamic response, but that the heat release fluctuations cannot be predicted, since no interaction between flow and reaction rate is taken into account.

4.1 Resolvent Analysis in the Linear Regime

The focus of the resolvent analysis in this section is on the effect of acoustic forcing on vortex shedding in a swirling jet in the linear regime. It is therefore assumed that the influence of

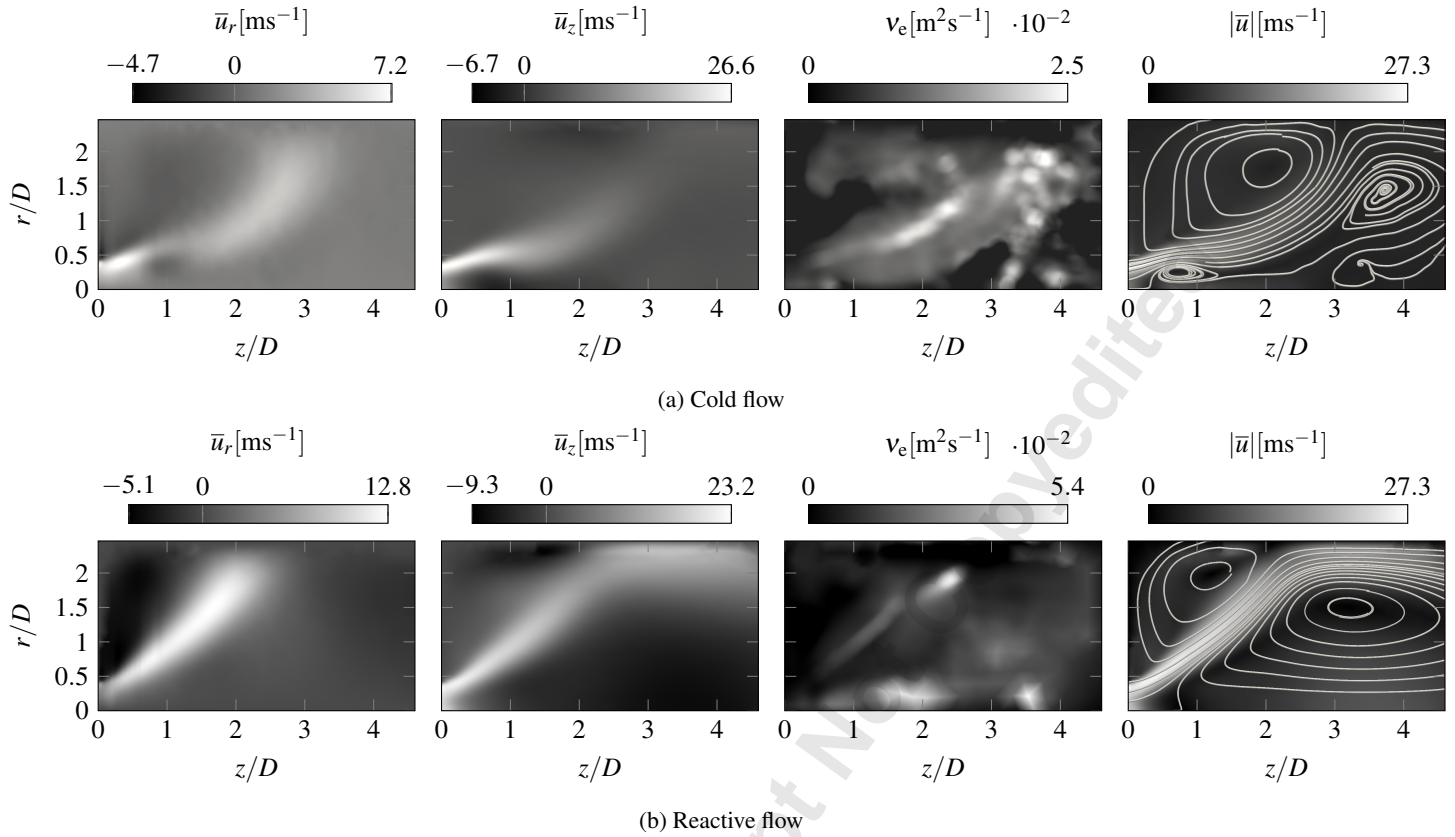


FIGURE 3: Velocity and eddy viscosity fields based on experimental PIV measurements for the cold flow case and the reactive case

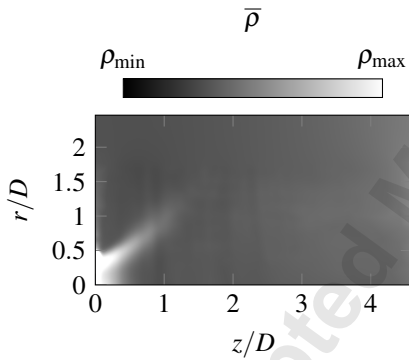


FIGURE 4: Mean density field for the same reactive flow as shown in Fig. 3b

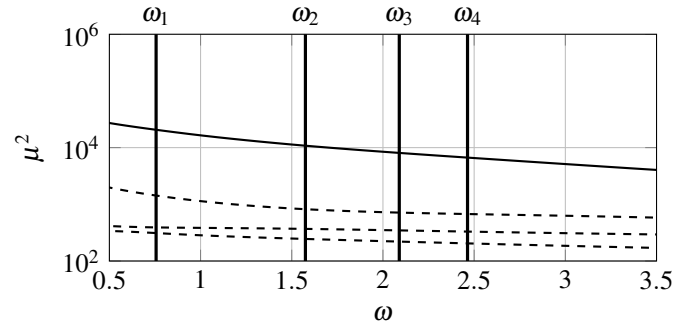


FIGURE 5: Resolvent analysis in the linear regime: the four highest resolvent gains μ^2 versus the experimental turbulent kinetic energy at the forcing frequency; dominant gain (—) and subdominant gains (---)

the coherent structures on the time-averaged flow (via modulation of the Reynolds stress tensor) and on the eddy viscosity is small enough to be neglected. Hence, both the time-averaged velocities and the thereupon based eddy viscosity obtained from the unforced flow, which are shown in Fig. 3a, serve as input for the resolvent analysis in this section. The results of the resolvent

analysis, i.e. the dominant optimal response, will be validated against FFT of time-resolved PIV snapshots. These snapshots were taken when the flow was simultaneously acoustically forced by a harmonic signal.

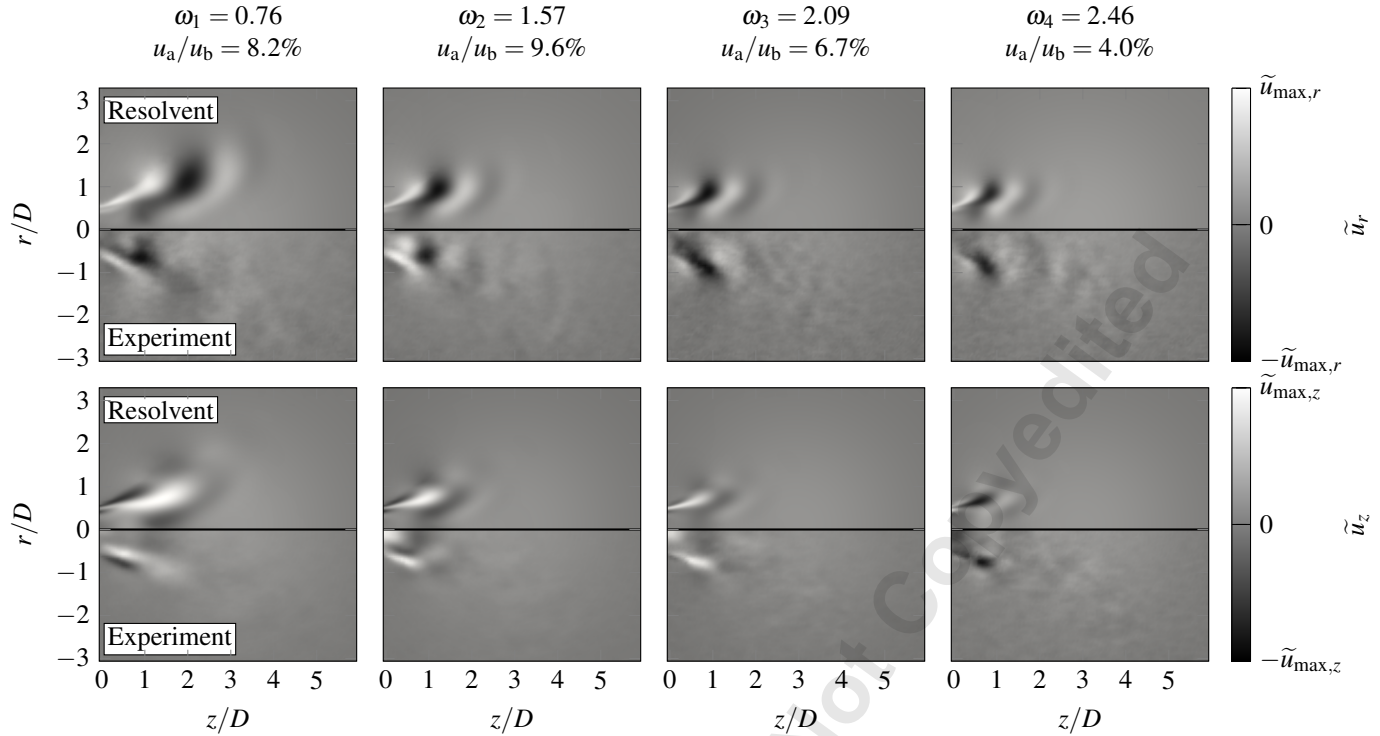


FIGURE 6: Velocity fields of the dominant optimal response, as obtained in the resolvent analysis in the linear regime (upper half plane) versus FFT of experimental PIV snapshots (lower half plane). Various frequencies are forced acoustically. The first row shows the radial velocity perturbation fields and the second row shows the axial velocity perturbation fields.

Figure 5 shows the four highest gains in the spectrum of the resolvent analysis. The graph demonstrates that one gain is dominant for all frequencies of interest, i.e. the pulsation frequencies in the experiment, which are indicated by the vertical lines in Fig. 5. We can therefore assume that the low-rank requirement is met and it is sufficient to focus on the dominant optimal response alone, while sub-dominant optimal response structures with lower gains may be neglected.

The optimal responses based on the resolvent analysis are compared in Fig. 6 to the measured Fourier modes. The acoustic velocity amplitudes range from $u_a/u_b = 4\%$ to $u_a/u_b = 9.6\%$ (The respective acoustic velocity amplitudes are also noted in Fig. 6 above the respective plots). The first row shows the radial velocity, while the second row displays the axial velocity component. The resolvent results are given in the upper half-plane, i.e. above the solid black lines, while the experimental results are shown in the lower half-planes. Especially at high frequencies, the experimental coherent structures are very well reproduced by the dominant optimal response obtained from resolvent analysis. At low frequencies, minor deviations occur, which are especially visible in the radial velocity component.

One explanation for the minor deviations between resolvent analysis and experimental Fourier modes could be caused by

fluctuating swirl (see e.g. Palies et al. [40]): we assume that the azimuthal mean velocity component has no significant effect, when the forcing of the flow is axisymmetric. However, swirl fluctuations, caused by the acoustic perturbation at the swirl generator upstream of the chamber, could impose an additional forcing. This effect would be included in the experimental Fourier modes, it is however currently not taken into account by the resolvent analysis.

Schimek et al. [41] measured swirl fluctuations in a different burner setup. They showed that the fluctuations are large at low frequencies and decrease at high frequencies. This is in line with the assumption that at low frequencies the swirl fluctuations should be taken into account to improve even more the results of the resolvent analysis.

4.2 Resolvent Analysis in the Non-Linear Regime

The results in the previous section showed that in the linear regime, the resolvent analysis predicts with high accuracy the coherent hydrodynamic structures that couple to the acoustic forcing. As it is well known, for strong forcing, non-linear effects become non-negligible and it must be verified if the linear approach yields accurate predictions. One non-linear effect

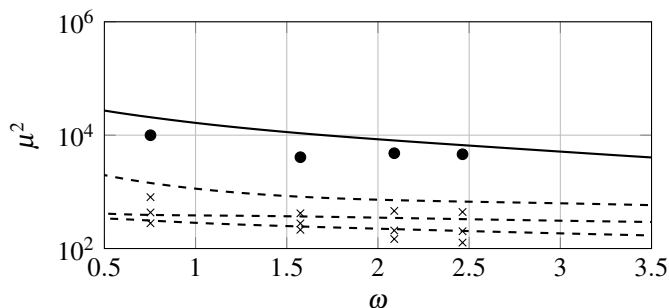


FIGURE 7: Resolvent Analysis in the non-linear regime: dominant (●) and first three subdominant gains (×). The lines correspond to the linear gains, also shown in Fig. 5

is the modulation of the mean flow due to the Reynolds stresses caused by the hydrodynamic structures. In order to take this effect into account in the resolvent analysis, it is not performed on the unperturbed time-averaged flow, i.e. the flow illustrated in Fig. 3a, but on the time-average of the acoustically forced flows. Changes in the field of eddy viscosity however are neglected here and the eddy viscosity field of the unforced flow is applied.

Figure 7 displays the resolvent gains for the four actuation frequencies that were used in the experiment. The plot shows that the strong acoustic perturbation has led to a significant saturation at all frequencies, such that the flow is less receptive to additional perturbation in comparison with the linear case. Since also the gain of the subdominant structures appears to be decreased by the strong forcing, the low-rank assumption still holds. Therefore, we expect that the experimental Fourier mode shapes are still well reproduced by the leading optimal response.

The velocity fields of the dominant optimal response in the non-linear regime are depicted in Fig. 8, together with the corresponding experimental Fourier modes. The coherent structures seen in the experimental velocity fields are reproduced with good accuracy by the resolvent analysis. Considering the very high acoustic velocity forcing amplitudes, which range between 46.5% and 68.6% of the bulk velocity, this agreement is quite remarkable.

In an attempt to stretch the linear resolvent analysis beyond its limit of validity, the experimental flow was finally forced with the maximal acoustic amplitude provided by our apparatus, which corresponds to 108% of the bulk speed at $\omega_1 = 0.76$. The resolvent analysis in this case yields a leading gain of $\mu_1^2 \approx 1.09 \cdot 10^4$, while the second highest gain is of $\mu_2^2 \approx 887$. Therefore, the low-rank requirement appears to be met also at

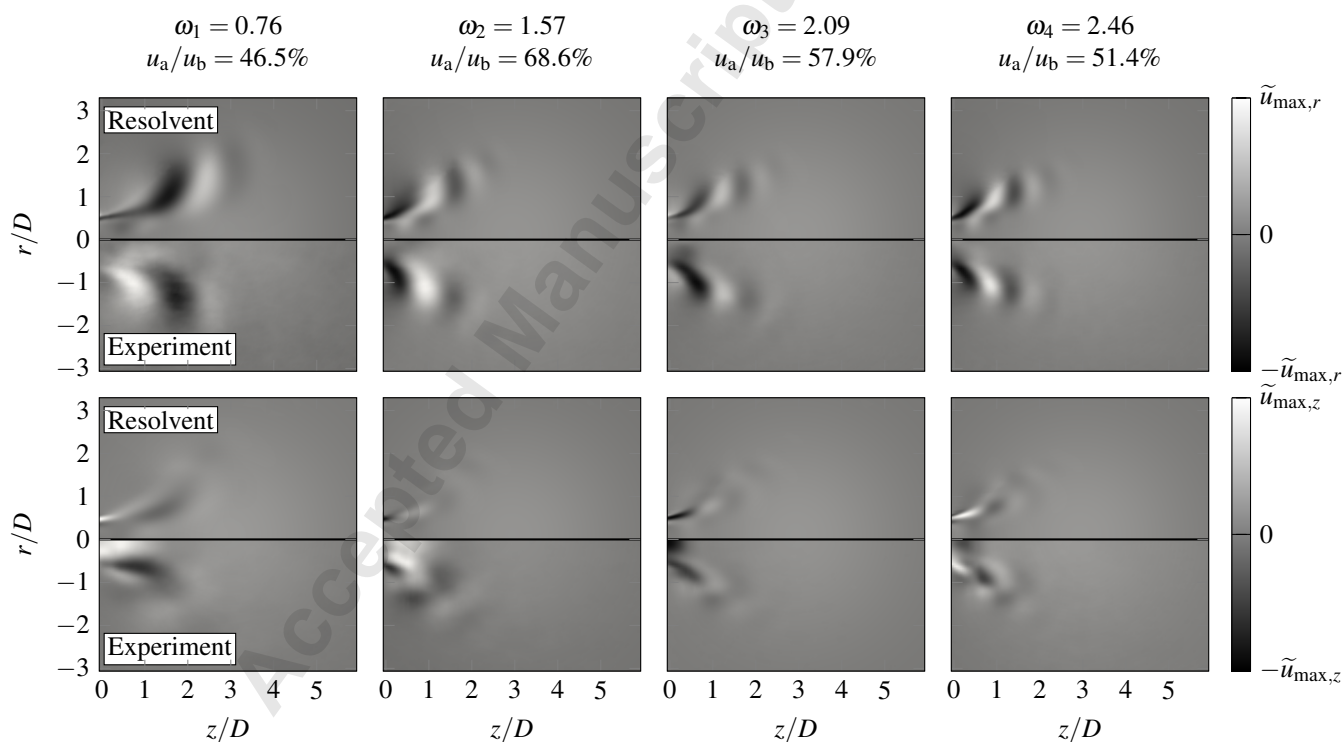


FIGURE 8: Velocity fields of the dominant optimal response as obtained in the resolvent analysis in the non-linear regime, versus FFT of experimental PIV snapshots. The arrangement is the same as in Fig. 6

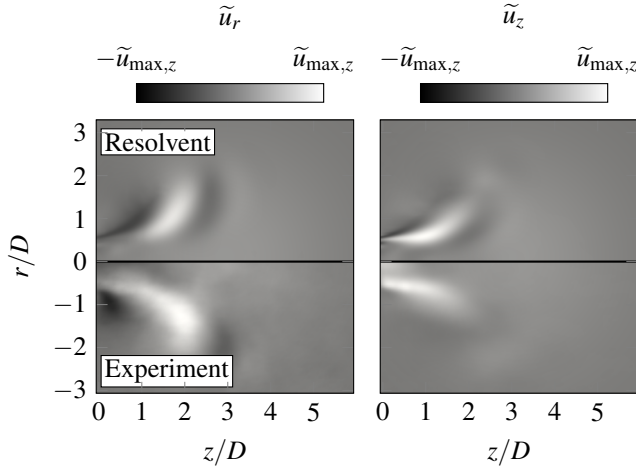


FIGURE 9: Dominant optimal response based on resolvent analysis versus experimental Fourier modes at very high forcing amplitudes ($u_a = 108\% u_b$) at $\omega_1 = 0.76$.

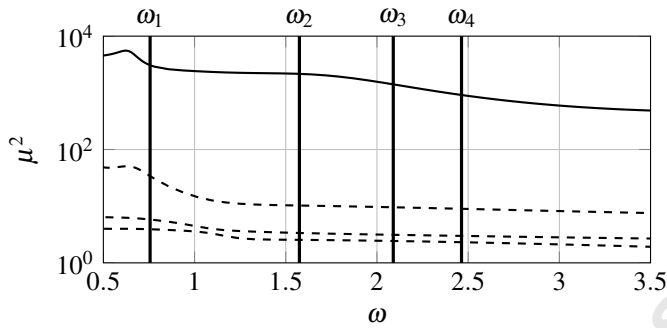


FIGURE 10: Resolvent analysis in the linear regime of the reacting flow: the four highest resolvent gains μ^2 versus the experimental turbulent kinetic energy at the forcing frequency; dominant gain (—) and subdominant gains (- - -)

these very high forcing amplitudes. Fig. 9 compares the dominant optimal response to the corresponding experimental Fourier modes. Despite a slightly underestimated wave length, which is best seen in the radial component, the spatial shapes of the coherent structures overall match. This was not expected considering the strong acoustic forcing.

4.3 Resolvent Analysis in Reacting Flows

Finally, the resolvent analysis is applied to a forced reacting flow, the mean flow of which is depicted in Fig. 3b and Fig. 4. The forcing amplitude is comparably low and we therefore assume that the flow shows a linear response to the acoustic forcing. The gains μ^2 for the linear case are shown in Fig. 10. Again

one dominant gain value stands out, while the subdominant gains are significantly lower. As in the cases analyzed above, this demonstrates that the system is of low rank, and the dominant optimal response of the resolvent analysis is hence expected to accurately describe the experimental Fourier modes.

The perturbation fields of the dominant optimal response are again shown alongside experimentally measured Fourier modes in Fig. 11. The Fourier mode shapes of radial velocity are reproduced with decent accuracy by the resolvent analysis. The same holds for the axial components at the lower frequencies. At $\omega = 2.46$, the discrepancies between the linear model and the experimental measurement have become quite marked. Concerning the fields of density fluctuation, the numerical results correspond surprisingly well to the experimental OH^* measurements. It may reasonably be assumed that without linearization of the reaction chemistry, the linear approach would not be able to capture the heat release fluctuations. Yet, especially at the lower frequencies, the density fluctuation obtained from the resolvent analysis agrees well with the OH^* -chemiluminescence fluctuations. Note here that a phase difference of $\pi/2$ between the density fluctuations and the OH^* fluctuations was assumed.

5 CONCLUSION

Resolvent analysis is applied to the flow field of a swirl-stabilized combustor, which is acoustically forced from upstream, in cold flow as well as in reacting operating conditions. Experimental measurements provide both the time-averaged flows, which serve as input for the resolvent analysis, and the validation basis for its results, i.e. the dynamic response to acoustic actuation.

It is shown that for low acoustic excitation in the linear regime, the flow shows low-rank behavior, i.e. the hydrodynamic response of the flow is captured by the dominant optimal response obtained from resolvent analysis. As a consequence, the dominant optimal response shows very good agreement with the Fourier modes of time-resolved experimental PIV snapshots. The results in the linear regime confirm the conclusion of McKeeon and Sharma [13] that in the case of low rank behavior the dominant optimal response based on the resolvent analysis governs the dynamic response of the flow.

Furthermore, the resolvent analysis is tested in the non-linear regime, i.e. with very high acoustic velocity amplitudes corresponding to between 46.5% and 68.6% of the bulk velocity. It was demonstrated that the high forcing amplitudes caused a decrease in relative difference between the dominant and the first subdominant gains, which however still remained significant. Therefore, a comparison between the dominant optimal response and the experimental Fourier modes still showed good agreement at these high forcing amplitudes. In order to test the limits of the resolvent analysis in this configuration, the method is furthermore applied to the highest possible forcing amplitude

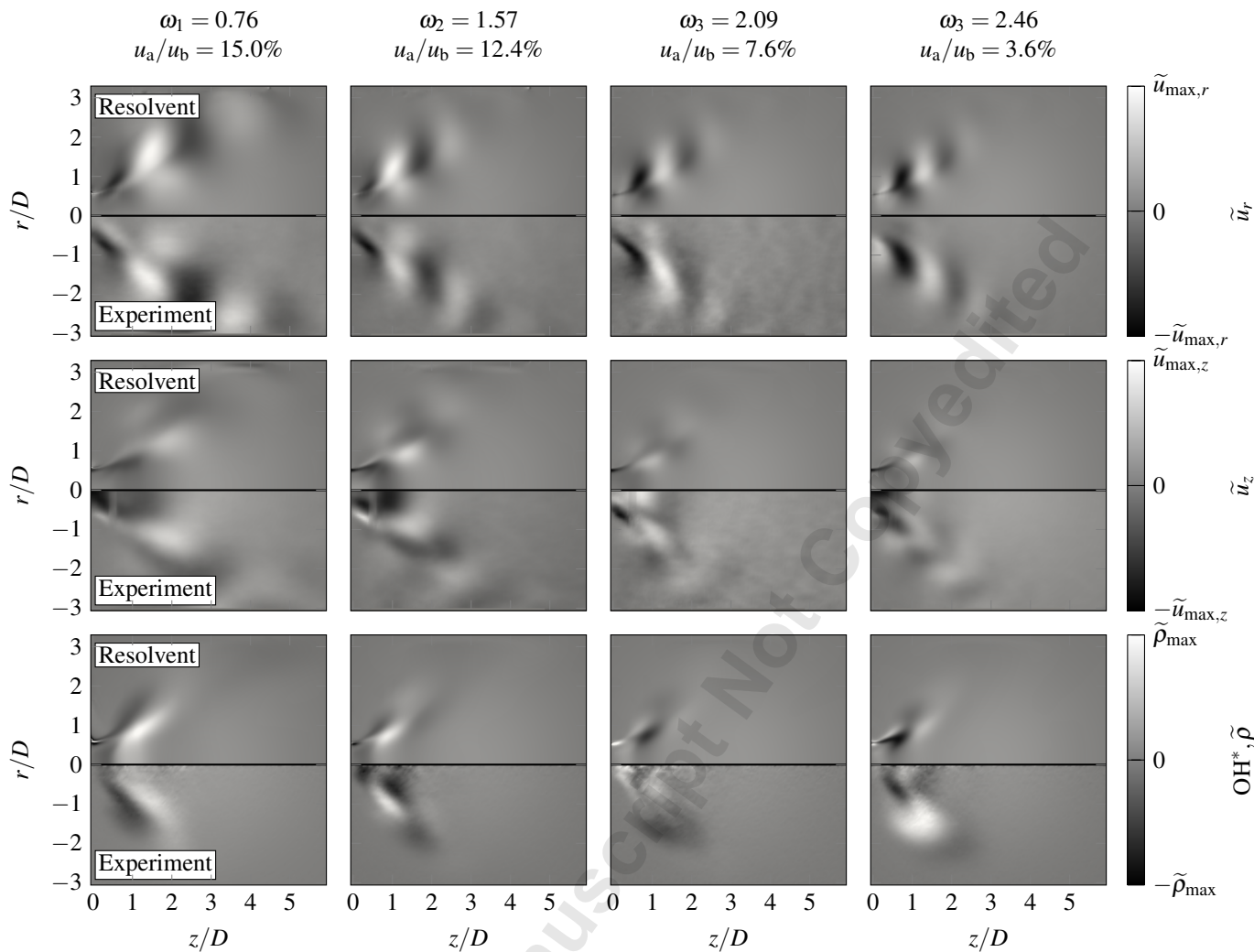


FIGURE 11: Velocity and density fields of the dominant optimal response as obtained in the resolvent analysis in the *reacting* case, versus FFT of experimental PIV snapshots. The arrangement is the same as in Fig. 6. The third row shows the density fluctuation versus the experimental OH^* measurements. Note here that a phase angle of $\pi/2$ between the OH^* measurements and the density was assumed.

of 108% of the bulk velocity. As both the dominant and the highest subdominant gains are decreased by the increased acoustic forcing levels, the flow still meets the low-rank condition. In this study, high forcing amplitudes never caused the low-rank condition to break down. A slight underestimation of the wave length in the optimal response suggests, however, that the approach is close to its application limit concerning the actuation amplitude. Nevertheless, the optimal response still compares favorably with the experimental Fourier modes, perhaps surprisingly so, in the presence of such strong acoustic forcing.

Finally, a reacting swirled flow is subject to the resolvent analysis. We show that in this case the leading gain is dominant over a wide range of frequencies. Considering the linear

regime, the velocity components of the dominant optimal response obtained by a resolvent analysis around the unperturbed mean flow agree well with the experimental observations. Although no chemistry model is included in the resolvent analysis, the density fluctuations display a remarkable resemblance to Fourier modes of the OH^* -chemiluminescence fluctuation at low frequencies. Our results suggest that, in this configuration, the flame response to acoustic forcing at low frequencies is dominated by hydrodynamic mechanisms, and that reaction chemistry is not significantly involved in the instability dynamics. The last conclusion of this proof of concept therefore is that the resolvent analysis is well applicable to reacting flows.

As a consequence of the successful proof of concept, this

paper underlines the capabilities of resolvent analysis and its potential for the combustion and gas-turbine community. As a subsequent step, a reaction model could be included in the linearized equations. This was recently done - however for laminar flames - by Avdonin et al. [42]. Extending this approach to turbulent flames might increase the quality of prediction of heat release fluctuations of the swirl flame. In this paper, it was demonstrated, that the resolvent analysis predicts the dynamic structures of the flow, but not their amplitude. Taking this into account would be a second logical next step in order to predict the entirety of the flow response to acoustic forcing and therefore to calculate FTFs from mean flow data.

ACKNOWLEDGMENT

The research leading to these results has received funding from the Deutsche Forschungsgemeinschaft (DFG) under project number OB 402/4-3.

REFERENCES

- [1] Poinot, T. J., Trounev, A. C., Veynante, D. P., Candel, S. M., and Esposito, E. J., 1987. "Vortex-driven acoustically coupled combustion instabilities". *Journal of Fluid Mechanics*, **177**, pp. 265–292.
- [2] Stöhr, M., Boxx, I., Carter, C. D., and Meier, W., 2012. "Experimental study of vortex-flame interaction in a gas turbine model combustor". *Combustion and flame*, **159**(8), pp. 2636–2649.
- [3] Docquier, N., and Candel, S., 2002. "Combustion control and sensors: a review". *Progress in energy and combustion science*, **28**(2), pp. 107–150.
- [4] Barkley, D., 2006. "Linear analysis of the cylinder wake mean flow". *EPL (Europhysics Letters)*, **75**(5), p. 750.
- [5] Terhaar, S., Oberleithner, K., and Paschereit, C. O., 2015. "ScienceDirect Key parameters governing the precessing vortex core in reacting flows : An experimental and analytical study". *Proceedings of the Combustion Institute*, **35**(3), pp. 3347–3354.
- [6] Tammsola, O., and Juniper, M. P., 2015. "Adjoint sensitivity analysis of hydrodynamic stability in a gas turbine fuel injector". In ASME Turbo Expo 2015: Turbine Technical Conference and Exposition, American Society of Mechanical Engineers, pp. V04AT04A057–V04AT04A057.
- [7] Kaiser, T. L., Poinot, T., and Oberleithner, K., 2018. "Stability and Sensitivity Analysis of Hydrodynamic Instabilities in Industrial Swirled Injection Systems". *Journal of Engineering for Gas Turbines and Power*, **140**(5), jan, pp. 51506–51510.
- [8] Tissot, G., Lajús Jr, F. C., Cavalieri, A. V., and Jordan, P., 2017. "Wave packets and orr mechanism in turbulent jets". *Physical Review Fluids*, **2**(9), p. 093901.
- [9] Palies, P., Durox, D., Schuller, T., and Candel, S., 2011. "Acoustic–convective mode conversion in an aerofoil cascade". *Journal of Fluid Mechanics*, **672**, pp. 545–569.
- [10] Schuller, T., Cuquel, A., Palies, P., Moeck, J., Durox, D., and Candel, S., 2012. "Modeling the Response of Premixed Flame Transfer Functions - Key Elements and Experimental Proofs". In *50th AIAA Aerospace Sciences Meeting including the New Horizons Forum and Aerospace Exposition*, Aerospace Sciences Meetings, American Institute of Aeronautics and Astronautics, jan.
- [11] Trefethen, L. N., Trefethen, A. E., Reddy, S. C., and Driscoll, T. A., 1993. "Hydrodynamic stability without eigenvalues". *Science*, **261**(5121), pp. 578–584.
- [12] Beneddine, S., Sipp, D., Arnault, A., Dandois, J., and Lesshafft, L., 2016. "Conditions for validity of mean flow stability analysis". *Journal of Fluid Mechanics*, **798**, pp. 485–504.
- [13] McKeon, B., and Sharma, A., 2010. "A critical-layer framework for turbulent pipe flow". *Journal of Fluid Mechanics*, **658**, pp. 336–382.
- [14] Yi, T., and Santavicca, D. A., 2009. "Forced flame response of turbulent liquid-fueled lean-direct-injection combustion to fuel modulations". *Journal of Propulsion and Power*, **25**(6), pp. 1259–1271.
- [15] Gentemann, A., Hirsch, C., Kunze, K., Kiesewetter, F., Sattelmayer, T., and Polifke, W., 2004. "Validation of flame transfer function reconstruction for perfectly premixed swirl flames". In ASME Turbo Expo 2004: Power for Land, Sea, and Air, American Society of Mechanical Engineers, pp. 501–510.
- [16] Kaiser, T., Ztarlik, G., Selle, L., and Poinot, T., 2018. "Impact of symmetry breaking on the flame transfer function of a laminar premixed flame". *Proceedings of the Combustion Institute*.
- [17] Fleifil, M., Annaswamy, A. M., Ghoneim, Z., and Ghoniem, A. F., 1996. "Response of a laminar premixed flame to flow oscillations: A kinematic model and thermoacoustic instability results". *Combustion and flame*, **106**(4), pp. 487–510.
- [18] Schuller, T., Durox, D., and Candel, S., 2003. "A unified model for the prediction of laminar flame transfer functions". *Combustion and Flame*, **134**(1-2), pp. 21–34.
- [19] Schmidt, O., Towne, A., Rigas, G., Colonius, T., and Brès, G., 2018. "Spectral analysis of jet turbulence". *Journal of Fluid Mechanics*, **855**, pp. 953–982.
- [20] Lesshafft, L., Semeraro, O., Jaunet, V., Cavalieri, A. V. G., and Jordan, P., 2018. "Resolvent-based modelling of coherent wavepackets in a turbulent jet". *arXiv preprint arXiv:1810.09340*.
- [21] Silva, C. F., Nicoud, F., Schuller, T., Durox, D., and Candel, S., 2013. "Combining a helmholtz solver with the flame describing function to assess combustion instability

- in a premixed swirled combustor”. *Combustion and Flame*, **160**(9), pp. 1743 – 1754.
- [22] Schuermans, B., Bellucci, V., and Paschereit, C. O., 2003. “Thermoacoustic modeling and control of multi burner combustion systems”. In ASME Turbo Expo 2003, collocated with the 2003 International Joint Power Generation Conference, American Society of Mechanical Engineers, pp. 509–519.
- [23] Emmert, T., Meindl, M., Jaensch, S., and Polifke, W., 2016. “Linear state space interconnect modeling of acoustic systems”. *Acta Acustica united with Acustica*, **102**(5), pp. 824–833.
- [24] Oberleithner, K., and Paschereit, C. O., 2016. Modeling Flame Describing Functions Based on Hydrodynamic Linear Stability Analysis.
- [25] Reichel, T. G., Goeckeler, K., and Paschereit, O., 2015. “Investigation of Lean Premixed Swirl-Stabilized Hydrogen Burner With Axial Air Injection Using OH-PLIF Imaging”. *Journal of Engineering for Gas Turbines and Power*, **137**(11), sep, pp. 111510–111513.
- [26] Willert, C. E., and Gharib, M., 1991. “Digital particle image velocimetry”. *Experiments in Fluids*, **10**(4), Jan, pp. 181–193.
- [27] Soria, J., 1996. “An investigation of the near wake of a circular cylinder using a video-based digital cross-correlation particle image velocimetry technique”. *Experimental Thermal and Fluid Science*, **12**(2), pp. 221 – 233.
- [28] Huang, H., Fiedler, H., and Wang, J., 1993. “Limitation and improvement of piv”. *Experiments in fluids*, **15**(4-5), pp. 263–273.
- [29] Terhaar, S., and Paschereit, C. O., 2012. “High-speed piv investigation of coherent structures in a swirl-stabilized combustor operating at dry and steam-diluted conditions”. In 16th International Symposium on Applications of Laser Techniques to Fluid Mechanics, Lisbon, Portugal, July, pp. 9–12.
- [30] Hussain, A. K. M. F., and Reynolds, W. C., 1970. “The mechanics of an organized wave in turbulent shear flow”. *Journal of Fluid Mechanics*, **41**(2), pp. 241–258.
- [31] Manoharan, K., and Hemchandra, S., 2015. “Absolute/convective instability transition in a backward facing step combustor: Fundamental mechanism and influence of density gradient”. *Journal of Engineering for Gas Turbines and Power*, **137**(2), p. 021501.
- [32] Hussain, A., and Reynolds, W., 1972. “The mechanics of an organized wave in turbulent shear flow. part 2. experimental results”. *Journal of Fluid Mechanics*, **54**(2), pp. 241–261.
- [33] Ivanova, E. M., Noll, B. E., and Aigner, M., 2012. “A Numerical Study on the Turbulent Schmidt Numbers in a Jet in Crossflow”. *Journal of Engineering for Gas Turbines and Power*, **135**(1), nov, pp. 11505–11510.
- [34] Pope, S. B., 2000. *Turbulent Flows*. Cambridge University Press.
- [35] Poinsot, T., and Veynante, D., 2005. *Theoretical and Numerical Combustion*, Vol. 28. 01.
- [36] Sipp, D., Marquet, O., Meliga, P., and Barbagallo, A., 2010. “Dynamics and control of global instabilities in open-flows: a linearized approach”. *Applied Mechanics Reviews*, **63**(3), p. 030801.
- [37] Hecht, F., 2012. “New development in FreeFem++”. *J. Numer. Math.*, **20**(3-4), pp. 251–265.
- [38] Garnaud, X., Lesshafft, L., Schmid, P. J., and Huerre, P., 2013. “The preferred mode of incompressible jets: linear frequency response analysis”. *Journal of Fluid Mechanics*, **716**, pp. 189–202.
- [39] Oberleithner, K., Paschereit, C. O., and Wagnanski, I., 2014. “On the impact of swirl on the growth of coherent structures”. *Journal of Fluid Mechanics*, **741**, pp. 156–199.
- [40] Palies, P., Durox, D., Schuller, T., and Candel, S., 2010. “The combined dynamics of swirler and turbulent premixed swirling flames”. *Combustion and Flame*, **157**(9), pp. 1698 – 1717.
- [41] Schimek, S., Ćosić, B., Moeck, J. P., Terhaar, S., and Paschereit, C. O., 2012. “Amplitude-dependent flow field and flame response to axial and tangential velocity fluctuations”. In Proc. ASME Turbo Expo 2012, no. ASME paper GT2012-69785.
- [42] Avdonin, A., Meindl, M., and Polifke, W., in press 2018. “Thermoacoustic analysis of a laminar premixed flame using a linearized reactive flow solver”. *Proceedings of the Combustion Institute*.